MATERIALS PHYSICS AND MECHANICS RESEARCH ARTICLE

Submitted: July 13, 2025 **Revised: September 30, 2025** **Accepted: October 30, 2025**

Work hardening behavior of AISI 321 austenitic stainless steel with different initial microstructures

M.S. Ghazani [1]✉, H.A. Rezai [2]

[1] Department of Materials Science Engineering, University of Bonab, Bonab, Iran

[2] Department of Materials Science Engineering, Sahand University of Technology, Tabriz, Iran

✉ m_shaban@ubonab.ac.ir

ABSTRACT

In the present investigation, different microstructures were obtained in AISI 321 austenitic stainless steel by cold rolling and subsequent annealing at different temperatures. The effect of initial microstructure on the work hardening behavior was analyzed using tensile analysis. At annealing temperatures of 700 and 800 °C, the stage I hardening is not apparent due to the high density of dislocations existed inside the austenite grains prior to tensile deformation. But the stage I hardening is seen in the ln(σ) ~ ln(ε) curves of the sample annealed at 900 °C and coarse grained one because the microstructures are consisted of equiaxed and dislocation free austenite grains. More detailed results were also obtained by differential Crussard-Jaoul analysis. This analysis indicated the occurrence of austenite to martensite transformation during tensile deformation of as received sample and that was annealed at 900 °C, which is distinguished by a positive slope in the ln(dσ/dε) vs. ln(ε) curves.

KEYWORDS

AISI 321 stainless steel • work hardening • cold rolling • annealing • tensile deformation

Citation: Ghazani MS, Rezai HA. Work hardening behavior of AISI 321 austenitic stainless steel with different initial microstructures. *Materials Physics and Mechanics*. 2025;53(5): 108–121.
http://dx.doi.org/10.18149/MPM.5352025_9

Introduction

For a work-piece to be suitable for utilization in a corrosive environment under external loads, the material used in its manufacture must have a combination of excellent corrosion resistance and outstanding mechanical properties [1]. Under these conditions, austenitic stainless steels are a good candidate. Despite these excellent properties, most of the austenitic stainless steels are susceptible to intergranular corrosion [2,3] and stress corrosion cracking [4]. In order to improve the resistance to intergranular corrosion and prevent sensitization, a sufficient amount of carbide forming elements such as titanium and niobium is added to their chemical composition. In Ti stabilized the AISI 321 austenitic stainless steel, a suitable amount of titanium (wt. %Ti =5 × wt. %C) is added to favor the formation of TiC precipitates which keeps chromium in solution at the austenite grain boundary area and improves resistance against the grain boundary sensitization [5].

Much research has been done on the corrosion resistance of this type of steel. For example, Lima et al. [6] studied the sensitization evaluation of austenitic stainless steels and reported that the stabilized steels (AISI 321 and AISI 347) are more resistant to sensitization than non-stabilized steels (ISI 304 and AISI 316). It was also concluded that niobium is more efficient stabilizing agent than titanium. Pardo et al. [7] studied the influence of Ti, C and N content of chemical composition on the intergranular corrosion

Publisher: Peter the Great St. Petersburg Polytechnic University

resistance of AISI 316Ti and AISI 321 stainless steels. It was demonstrated that the addition of Ti promotes intergranular corrosion resistance in stainless steels. Also, the reduction of carbon content to below 0.03 wt. % increases the sensitization resistance more than does Ti content.

Some research has also been done on the mechanical properties of the AISI 321 austenitic stainless steel. Zhao et al. [8] investigated the effect of solution treatment on microstructures and mechanical properties of the AISI 321 steel. They reported that the amount of sigma phase in the microstructure reaches to 18 wt. % after 1000 h service at 800 °C. It was concluded that the amount of sigma phase decreases from 18 to 2.6 wt. % with increasing the duration of solution annealing to 2 h. Also, it was shown that the size of austenite grains increases with solution annealing time which improves the fracture toughness in AISI 321 stainless steel. The strain hardening capacity measured by tensile testing is one of deformation characteristics of materials which determines the amount of uniform plastic deformation [9,10]. In materials with low strain hardening exponent, the onset of necking occurs earlier, and the total elongation and ductility decreases during tensile deformation [11]. This parameter also affects the toughness and workability of materials during metal forming processes. Dini et al. [12] investigated the effect of grain size on the work hardening behavior of high manganese austenitic steel and demonstrated that the optimum mechanical properties are achieved with varied work hardening capacities that can be obtained by changing the grain size. Also, it has been approved that the main reason for the low ductility of nanostructured materials is the low work hardening rate during uniform plastic deformation stage [13]. Therefore, Wang et al. [14] proposed three different strategies to achieve uniform tensile deformation in nanostructured metals. Producing bimodal or multi-modal grain size distribution is one of these methods. Considering the available literature, it is observed that the work hardening behavior of the AISI 321 stainless steel has been studied only in the work of Zhang et al. [15]. In this investigation, the difference in the work hardening behaviors of AISI 321 and Hadfield steels were attributed to the occurrence of twining in the Hadfield steel. Also, they declared that work hardening of the AISI 321 stainless steel is mainly resulted from dislocation interactions. They did not report any other microstructural evolution, such as austenite to martensite transformation (TRIP effect), that can affect the work hardening behavior of this steel. It is to be mentioned that our previous work [16] was mostly focused on post-deformation annealing's role on microstructure and mechanical properties of the cold-rolled AISI 321 stainless steel. In contrast, this work reports a thorough and detailed investigation of work hardening behavior by both Hollomon and differential Crussard–Jaoul (C–J) methods. In addition, the impact of different initial microstructures (coarse-grained, fine-grained, bimodal, and cold-worked) on absence or presence of visible hardening steps is described and the role of austenite-to-martensite transformation is highlighted (TRIP effect). These points have not been expressed in the literature and constitute the innovation of this study.

Materials and Methods

The chemical composition of the AISI 321 austenitic stainless steel used in the present study is represented in Table 1. In this type of stainless steels, chromium and nickel are

added to increase the corrosion resistance and stabilize the austenite phase respectively. Moreover, the addition of titanium by 0.3 wt. % prevents the sensitization of material to grain boundary corrosion through the formation of titanium carbide (TiC) precipitates instead of chromium carbide ($Cr_{23}C_7$) which depletes grain boundaries from chromium. The material was received in the form of a sheet with 10 mm thickness. The sheet was cut into smaller pieces with dimensions of 150 × 25 mm^2 to be suitable for cold rolling. All pieces were solution annealed at 1200 °C for 15 min and then quenched in water to obtain a fully austenitic structure. All samples were then rolled at room temperature with 80 % cross-section reduction. After cold rolling, samples were annealed for 15 min at 700, 800, and 900 °C.

Table 1. Chemical composition of the AISI 321 austenitic stainless steel

C	Si	Mn	Cr	Ni	Mo	Ti	N	Fe
0.036	0.421	1.910	17.154	8.620	0.374	0.303	0.013	bal.

Microstructure analysis was performed using optical microscopy after surface preparation by conventional metallographic procedure. For this reason, sample surfaces were ground with sandpapers of 100–2500 grit and then mechanically polished with 0.05-μm alumina suspension. To reveal grain structure, the electrolytic etching was used in the solution of 50 % nitric acid and distilled water by applying the current density of 0.1 mA/cm^2. Optical images were taken using Olympus PMG3 microscope. Tensile testing at room temperature was used for analyzing mechanical properties and work hardening behavior of cold rolled and annealed samples. Tensile samples were prepared according to ASTM E8 standard and tensile tests were conducted using Gotech AI-7000-LA20 testing machine with the cross-head speed of 0.1 mm/min. The work hardening behavior of cold rolled and annealed samples were then analyzed employing the Hollomon and differential C-J methods.

Results and Discussion

Tensile properties

Figure 1(a) shows the engineering stress-engineering strain curves of the AISI 321 austenitic stainless steel at different annealing conditions. As can be seen, the as received sample exhibit a lower tensile stress and higher elongation than the cold rolled and subsequently annealed samples. Also, exceptionally high value of tensile elongation observed during tensile testing as received sample, can be attributed to microstructural evolutions during deformation, and will be discussed later. For annealed samples, it is seen that the tensile strength increases and elongation to failure decreases with decreasing annealing temperature. The true stress-true strain curves obtained from engineering curves are shown in Fig. 1(b). These curves were plotted up to the strain corresponding to the maximum stress in the engineering stress-engineering strain curves. Obtained true stress-true strain curves were then used for evaluation of the work hardening behavior of the AISI 321 steel during tensile deformation. The tensile properties of the AISI 321 austenitic steel at different annealing conditions, obtained from engineering curves, are summarized in Table 2. The yield and tensile strengths of as received sample are 92 and 439 MPa respectively. The yield strength of as-received

sample is increased from 92 to 330, 586, and 800 MPa after cold rolling and annealing at 900, 800, and 700 °C respectively. Also, the tensile strength increases from 439 to 668, 956, and 1189 MPa by cold rolling and annealing at 900, 800, and 700 °C, respectively. The variations of tensile properties by cold rolling and annealing could be discussed considering the obtained microstructures.

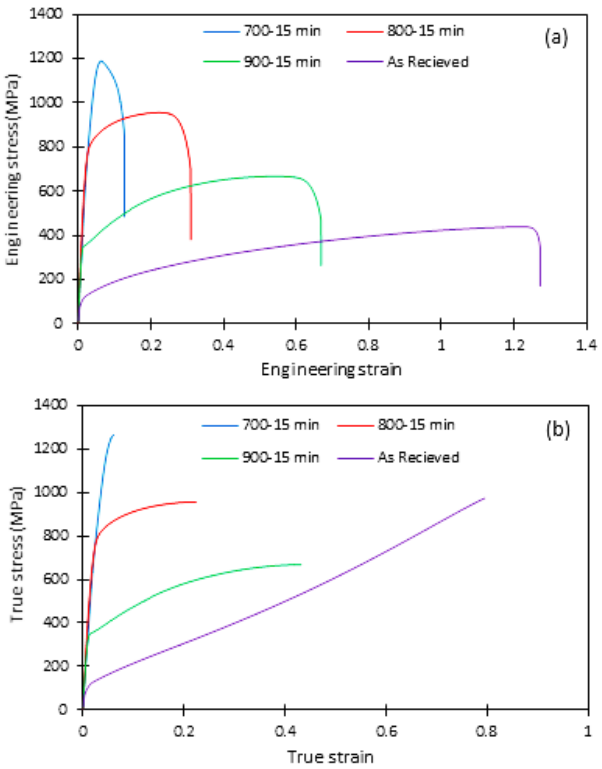

Fig. 1. Engineering stress vs. engineering strain (a), and true stress vs. true strain (b) curves of AISI 321 austenitic stainless steel after cold rolling and annealing at different temperatures

Table 2. Tensile properties of the as-received and cold rolled and annealed AISI 321 steels

Sample	Yield strength	Tensile strength	Total elongation, %	Uniform strain	Non-uniform strain	Hardening capacity	Uniform/non-uniform
700 °C	800 ± 12	1189 ± 20	13 ± 1	0.06	0.07	0.49	0.86
800 °C	586 ± 16	955 ± 13	31 ± 2	0.24	0.06	0.63	3.77
900 °C	330 ± 10	667 ± 12	67 ± 4	0.59	0.08	1.02	7.37
As-received	92 ± 8	439 ± 9	127 ± 6	1.23	0.04	3.78	30.75

Figure 2 shows the optical micrographs of the as-received and cold rolled and annealed samples. It is seen that the initial microstructure (Fig. 2(d)) is consisted of equiaxed austenite grains where their mean size was measured to be 120 μm with average intercept method. Fig. 2(c) shows the microstructure of the AISI 321 steel after cold rolling and annealing at 900 °C. This microstructure is also consisted of equiaxed austenite grains with the mean grain size of 5 μm. This uniform microstructure is obtained due to the occurrence of three different phenomena during annealing: static recrystallization in cold deformed austenite grains, martensite to austenite reversion and subsequent grain growth. The increase in strength after cold rolling and annealing at

900 °C is attributed to the reduction of mean grain size of austenite from 120 to 5 μm. It should be emphasis that the grain size strengthening follows the Hall-Petch relation in which the yield strength is proportional to the inverse of the square root of mean grain size ($\sigma_y = \sigma_0 + kd^{-1/2}$). According to Hall-Petch relation, the strength of material increases with decreasing grain size. It is worth to note that the number of dislocations at pile-ups decreases with grain refinement which produces smaller strain concentrations at the boundary with the nearing grain. Therefore, higher applied stresses are required to cause slip to pass to the neighboring grains through the grain boundary [17].

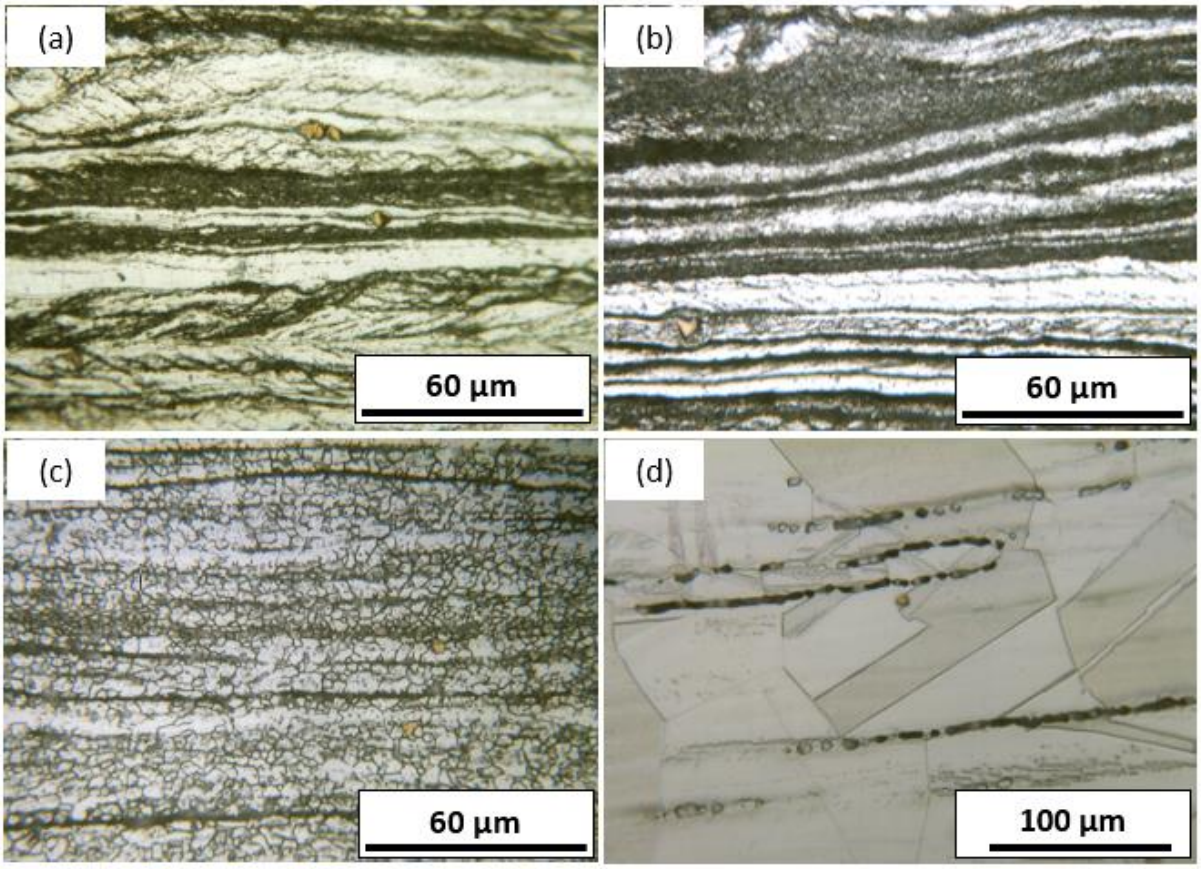

Fig. 2. Optical microstructures of AISI 321 austenitic stainless steel after cold rolling and annealing for 15 min at different temperatures: (a) 700 °C, (b) 800 °C, (c) 900 °C, and (d) initial coarse-grained sample

Figure 2(b) shows the microstructure after cold rolling and annealing at 800 °C for 15 min. The microstructure appears to consist of elongated austenite grains, together with ultrafine austenite grains formed by martensite reversion. The presence of relatively equiaxed and bright regions suggests that partial recrystallization might have occurred locally, although this cannot be confirmed with certainty using only optical metallography. Advanced characterization (e.g., electron backscatter diffraction (EBSD) or transmission electron microscopy (TEM)) would be necessary to unambiguously verify recrystallization. At this condition, the annealing time and temperature is probably not high enough for the sufficient growth of the ultrafine austenite grains, so that the bimodal grain size is produced. Whereas, annealing at 900 °C results in a uniform microstructure may be due to the intense growth of ultrafine austenite grains, after the martensite to

austenite phase transformation, so that their sizes are almost become equal to the mean size of the coarse austenite grains obtained by static recrystallization. Therefore, it could be mentioned that the increase in yield strength from 330 to 568 MPa and tensile strength from 668 to 956 MPa with decreasing the annealing temperature from 900 to 800 °C is mainly due to the refinement of equiaxed austenite grains. As it is seen in Fig. 2(a), the microstructure after annealing at 700 °C for 15 min is consisted of ultrafine austenite grains (dark regions) developed as a result of martensite to austenite transformation and elongated austenite grains (bright regions) with the traces of shear bands which indicates that the annealing temperature is not high enough to trigger static recrystallization inside cold worked grains. Therefore, increasing yield strength to 800 MPa and tensile strength to 1189 MPa by annealing at 700 °C is due to the effect of grain refinement and also higher dislocation density inside the elongated grains.

Hollomon analysis of work hardening behavior

In the present study, the Hollomon power low expression was used to describe the strain hardening characteristics of the AISI 321 austenitic stainless steel at different annealed conditions. The Hollomon equation is as follows [18]:

$$\sigma = k\varepsilon^n, \quad (1)$$

where ε is true strain, σ is true stress, n is the strain hardening exponent, and k is the strength coefficient. As it is evident, by writing the logarithmic form of the above equation, it is possible to evaluate the strain hardening exponent (n) and the strength coefficient (k) from the slope and intercept of the curves, respectively. The logarithmic form of the Hollomon equation is written as below:

$$ln\,(\sigma) = ln\,(k) + n\,ln\,(\varepsilon). \quad (2)$$

Figure 3 shows the ln (σ) vs. ln (ε) curves obtained from the experimental true stress vs. true strain curves of the as received and the cold rolled and subsequently annealed samples. The obtained plots indicate that none of the samples exhibited the linear variation of the ln(σ) vs. ln(ε) with a unique value for strain hardening exponent (n). As can be seen, for samples annealed, after 80 % cold rolling, at 700 and 800 °C for 15 min, the two-stage work hardening behavior is evident where the value of work hardening exponent is higher at first stage compared with second stage (Fig. 3(a,b)). Also, for sample annealed at 900 °C for 15 min after cold rolling and as received coarse grained one, the two-stage work hardening behavior is obvious (Fig. 2(c,d)) but the strain hardening exponent in the second stage is higher than the first stage. The two-stage work hardening behavior of steels has been reported earlier by other researchers. Shin et al. [19] studied the variation of tensile behavior after aging heat treatment of precipitation hardened martensitic steel. They suggested that the plastic strain regimes can be divided into two different stages by a rapid increase in strain hardening followed by a comparatively lower increase. It was revealed in their investigation that the strain hardening exponents at the first and the second stages is associated with the Ni_3Al precipitates. Kosaka et al. [20] investigated the work hardening behavior of the ferritic steels containing fine carbides varied from 3 to 15 nm. They concluded that work hardening proceeds in two stages and the plastic strain at which the later stage starts during tensile deformation decreases with the increase in the diameter of carbides. It is worth to note that work hardening in FFC single

crystal materials occurs in three different stages based on the nature of the dislocation interactions during tensile deformation. Comparing the results obtained in this study with the work hardening behavior of FCC materials [21], it is inferred that the stage I is absent during tensile testing of all samples. It should be noted that the stage I work hardening is representative of the easy glide of dislocations at the beginning of plastic deformation of single crystal materials. At this step, dislocations can slip over a long distance on the primary slip system without interacting with other dislocations and obstacles. The stage I work hardening is characterized by the low values of strain hardening exponent. Whereas the stage I work hardening shown in Fig. 3(c,d) for sample annealed at 900 °C for 15 min and as received coarse gained one does not occur due to easy glide of dislocations. For polycrystalline materials such as the present steel, the initial stage of deformation is more appropriately attributed to early multiple slip, which provides deformation compatibility between grains, rather than easy glide on a primary slip system as in single crystals. The low strain hardening rate observed in the stage I of the present samples is therefore interpreted as resulting from limited dislocation interactions at the onset of multiple slip, prior to significant dislocation accumulation and forest hardening.

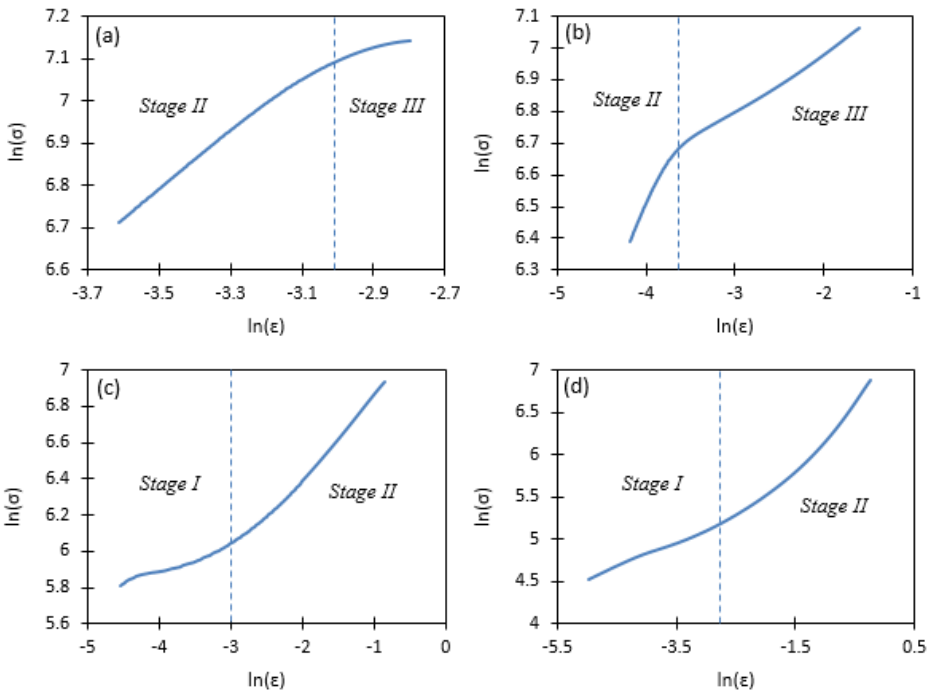

Fig. 3. ln(*σ*) vs. ln(*ε*) curves of the AISI 321 stainless steel after 80 % cold rolling and annealing for 15 min at temperatures of (a) 700 °C, (b) 800 °C, (c) 900 °C, and (d) the as received coarse grained sample in the annealed condition

As it is seen in Fig. 2(a), annealing at 700 °C for 15 min is not enough to transform the cold worked microstructure with high dislocation densities to the recrystallized and dislocation free austenite grains. Therefore, the dislocation tangles inside elongated grains may become an obstacle for generated dislocations during tensile testing which results in high levels of strain hardening at the initial stage of tensile deformation and the absence of the stage I work hardening. Also, some ultrafine austenite grains are evident in the primary elongated austenite grain boundaries which are the result of martensite to

austenite transformation. These ultrafine grains are also contributed in the high work hardening rate as previously reported by Del Valle et al. [22] for magnesium alloys processed by equal channel angular pressing. For sample annealed at 800 °C, Fig. 2(b), microstructure before tensile testing is composed of ultrafine, cold worked, and recrystallized austenite grains. In this case, the cold worked austenite and ultrafine equiaxed grains are responsible for the absence of the stage I work hardening. Whereas, for sample annealed at 900 °C for 15 min after cold rolling and initial coarse grained one, which has been annealed at 1200 °C, microstructures just before tensile testing are consisted of equiaxed dislocation free austenite grains due to the occurrence of static recrystallization and grain growth. In this case, the dislocation density inside grains is very low. For these two samples (coarse and equiaxed grain structure), the stage I of work hardening accompanies by the initiation of the stage II work hardening when the dislocation density inside each austenite grain increases and act as an obstacle for generated dislocations during continued deformation. Therefore, in the stage II, work hardening increases rapidly due to the interactions between dislocations on the activated secondary slip systems and those on the primary slip systems. A similar trend was observed during tensile deformation of the annealed AISI 321 and Hadfield steels in the work conducted by Zhang et al. [16]. For samples annealed at 700 and 800 °C, high density of dislocations which already existed inside elongated austenite grains, become an obstacle for generated dislocations so that the deformation process initiates from stage II hardening.

Table 3. Extracted data from the plots of $\ln(\sigma)$ vs. $\ln(\varepsilon)$ curves for the as received and annealed AISI 321 austenitic stainless steel

Annealing temperature, °C	Stage I	Stage II	Stage III	n_{I}	n_{II}	n_{III}	$\varepsilon_{I,II}$	$\varepsilon_{II,III}$
700	-	$\ln(\sigma)=0.6649\ln(\varepsilon)+9.1199$	$\ln(\sigma)=0.1559\ln(\varepsilon)+7.5798$	-	0.66	0.16	-	0.0485
800	-	$\ln(\sigma)=0.5715\ln(\varepsilon)+8.7936$	$\ln(\sigma)=0.1896\ln(\varepsilon)+7.3613$	-	0.57	0.19	-	0.0235
900	$\ln(\sigma)=0.1046\ln(\varepsilon)+6.3101$	$\ln(\sigma)=0.4663\ln(\varepsilon)+7.3222$	-	0.1	0.47	-	0.060	-
As-received	$\ln(\sigma)=0.271\ln(\varepsilon)+5.9037$	$\ln(\sigma)=0.8241\ln(\varepsilon)+7.0103$	-	0.27	0.82	-	0.135	-

The stage III work hardening initiates when the dislocation density inside grains reaches a critical value and the annihilation of dislocations by recovery become significant so that the work hardening rate decreases with further straining. For samples annealed at 700 and 800 °C, stage III work hardening is observed because the high density of dislocations exists prior to tensile deformation and further straining in the stage II increases dislocation density to a level that dislocation annihilation become predominant. But for sample annealed at the temperature of 900 °C and initial coarse grained one, dislocation density at the beginning of tensile deformation is very low and after the stage I (limited dislocation interactions at the onset of multiple slip) and stage II, remains in the lower levels so that the dislocation annihilation processes become insignificant compared with work hardening processes leading to the absence of the stage III work hardening. In Table 3, the results extracted from the $\ln(\sigma)$ vs. $\ln(\varepsilon)$

curves are represented, which include the work hardening exponent at different stages of work hardening and corresponding transition strains.

Differential C-J analysis of work hardening behavior

Here, it is useful to emphasis that the change in the deformation mechanisms during tensile testing of materials results in the development of different stages in the true stress-true strain curves. In the case of the single crystals of FCC materials, as previously mentioned, variations of the true stress (σ) with true strain (ε) shows three distinct stages in the uniform plastic deformation region [23]. These stages are the stage I, stage II and stage III of work hardening which relate respectively to the easy glide of dislocations on primary slip systems, high work hardening rate due to the activation of secondary slip systems, and the dynamic recovery of dislocations. Nevertheless, the changes in the deformation stages have not always an obvious effect on the tensile curves of polycrystalline materials. In this case, some forms of analysis are required to reveal different deformation stages using the data acquired from the rue stress- true strain curves [24]. Hollomon analysis in the previous section is the simplest of these methods. This analysis was previously used for prediction of the deformation stages in ferrite-martensite dual phase steel [25], but results showed a continuous decrease in the work hardening exponent (n) with strain and district stages was not revealed. Similar results were also reported by Umemoto et al. [26] for ferritic, martensitic, and bainitic single structure steels. In the present investigation, although the variations of the strain hardening exponent (n) with strain is near continuous (as seen in Fig. 3), but deformation stages can be approximately deduced from these plots. For precise analysis of the tensile stress- strain curves, the Crussard-Jaoul (C-J) method has been applied to many kinds of alloys and reasonable results have been obtained [25,27,28]. The differential C-J analysis of the work hardening behavior of materials is based on the Ludwik equation as below [29]:

$$\sigma = \sigma_0 + k_L \varepsilon^{n_L}, \tag{3}$$

where σ is true stress, ε is true strain, n_L is work hardening exponent, k_L and σ_0 are material constants. After differentiation, the above equation can be written as follows:

$$ln\left(\frac{d\sigma}{d\varepsilon}\right) = ln(k_L n_L) + (n_L - 1)\ln\varepsilon. \tag{4}$$

Before analyzing the tensile true stress- true strain curves using the differential C-J method, it should be mentioned that the ln(dσ/dε) vs. ln(ε) curves for polycrystalline materials comprises four distinct stages as reported by Reed-Heel et al. [30] for polycrystalline nickel. The typical form of the ln(dσ/dε) vs ln(ε) curves for polycrystalline materials with different stages is shown in Fig. 4. During the initial accommodation stage, multiple slip starts at largest grains and spreads in to finer grains with further straining. The stage I begins when all grains deform simultaneously by multiple slip. Therefore, the slope of the ln(dσ/dε) vs. ln(ε) curves increases when the stage I initiates. It is worth to note that stage I in the description of the work hardening behavior of poly-crystals differs fundamentally from the stage I of single crystals where the crystal deforms by easy glide of dislocations on primary slip system. In the stage II dislocation slip occurs on a single slip system with hardening effect of the dislocations on the secondary systems [31]. During this stage, the in-grain subdivision is a predominant phenomenon. It is worth

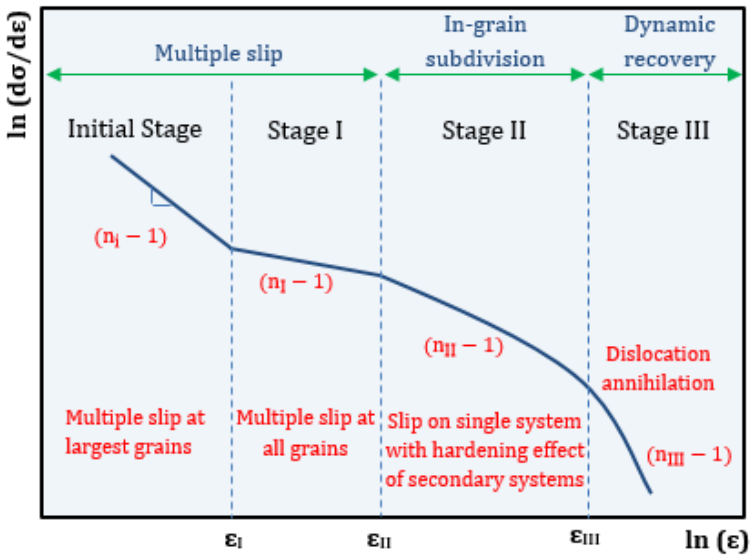

Fig. 4. Typical form of the ln(dσ/dε) vs. ln(ε) curves for polycrystalline materials. Based on [30]

to note that grain subdivision inside large austenite grains is primarily driven by multiple slip activity, which ensures deformation compatibility and promotes the gradual formation of dislocation substructures and misoriented sub-boundaries. This process is not confined to a particular stage of work hardening but occurs continuously from the very early stages of deformation until ultrafine-grained structures are eventually formed. The slope of the ln(dσ/dε) vs ln(ε) curve decreases when stage II initiates. Similar to work hardening behavior of single crystals, stage III is characterized by the occurrence of dynamic recovery due to the annihilation of dislocations. So, the slope of the ln(dσ/dε) vs. ln(ε) curve decreases when the stage III starts.

The differential C-J analysis of the true stress- true strain data for annealed samples was carried out using the Ludwik equation and the results are shown in Fig. 5. For the sample annealed at 700 °C for 15 min, as seen in Fig. 5(a), the three-stage hardening behavior is detected. Inspection of the microstructures of annealed samples in Fig. 2 reveals that after 15 min annealing at 700 °C (Fig. 2(a)), the microstructure is mainly composed of elongated austenite grains with cold deformed characteristics and some ultra-fine grains resulted from the reversion of deformation induced martensite. It is also obvious that the fraction of ultrafine-grained austenite is much less than the fraction of elongated grains where the occurrence of recovery is expected during annealing. As it is clear, the initial work hardening stage is not observed in the ln(dσ/dε) vs. $n\varepsilon$ curve of the sample annealed at 700 °C. This stage is observed when the initial microstructure of tensile sample is consisted of equiaxed grains with normal size distribution. The initial stage occurs with lower work hardening characteristics when the multiple slip starts only at larger grains. This stage accompanied with the stage I hardening when multiple slip occurs at all grains simultaneously. As the microstructure mainly consisted of cold deformed grains with high dislocation density which arranged in pileups, the initial stage is not observed and deformation starts with the occurrence of multiple slip at the elongated grains resulting to the stage I hardening.

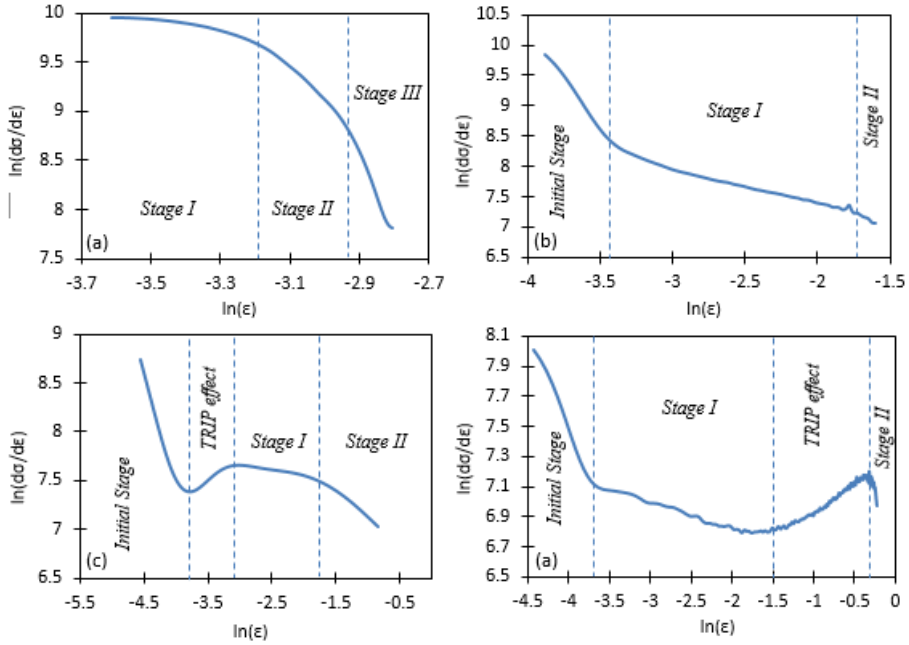

Fig. 5. Differential C-J analysis of the true stress-true strain curves of the AISI 321 austenitic stainless steel after annealing for 15 min at different temperatures: (a) 700 °C, (b) 800 °C, (c) 900 °C, and (d) initial coarse-grained steel

During the stage II, grain subdivision is predominant at elongated grains and also deformation of - ultra-fine austenite grains start with increasing the tensile stresses. As the work hardening capacity declines with grain refinement, the work hardening rate decreases in the stage II compared with the stage I. Finally, the stage III initiates when the dislocation annihilation occurs inside grains and work hardening rate decreases (Fig. 5(a)). For the sample annealed at 800 °C, as shown in Fig. 5(b), the ln(dσ/dε) vs. ln(ε) curve comprises three different stages. Comparing this curve with Fig. 3, it is deduced that the initial stage occurs with the characteristics of the multiple slip in large grains and accompanies with the stage I of work hardening due to the occurrence of multiple slip in all grains. This work hardening characteristics can be verified considering the initial microstructure of tensile sample (Fig. 2(b)). As said in the previous section, the microstructure after annealing at 800 °C is consisted of elongated austenite regions with the recrystallized features and also ultra-fine austenite grains due to the reversion of deformation induced martensite. Comparing this microstructure with Fig. 2(a), it is concluded that the size and volume fraction of ultra-fine austenite grains are increased with increasing the annealing temperature. Also, the static recovery inside elongated austenite grains is replaced by static recrystallization. In the presence of large austenite grains with low dislocation densities, due to static recrystallization, in conjunction with the ultra-fine grains, the plastic deformation starts with initial stage (high decrease rate of the work hardening) and accompanies with the stage I hardening, where the plastic deformation occurs simultaneously in ultra-fine and recrystallized austenite with different grain sizes.

Finally, the stage II hardening initiates at the final stage of the uniform plastic deformation region. This stage is characterized by the predominance of the subdivision of large austenite grains in the recrystallized regions (Fig. 2(b)) with the occurrence of single slip. So, the work hardening rate decreases in the stage II compared with

the stage I. As shown in Fig. 2(c,d), for samples annealed at 900 °C and initial coarse grained one, the trend similar to the behavior of the sample annealed at 800 °C is observed with this exception that the increase in the work hardening rate is noticed in some portion of the ln(dσ/dε) vs. ln(ε) curves. This increase in the rate of work hardening is attributed to the transformation of austenite phase to martensite during tensile testing which is known as TRIP effect.

Similar behavior has been reported by Cai et al. [32] for transformation induced plasticity (TRIP) steel with the chemical composition of Fe-0.18C-11Mn-3.8Al. They also explained that the superior tensile ductility is achieved in TRIP steels when the occurrence of austenite to martensite transformation is delayed. As can be seen in Fig. 5(c) the austenite to martensite transformation (TRIP) occurs in the early stage of uniform plastic deformation region for sample annealed at 900 °C. But for initial coarse-grained sample (Fig. 5(d)) this transformation is delayed and occurs in the later stage of the uniform plastic deformation region. This difference is attributed to the difference in the mean grain size of the austenite phase before the occurrence of TRIP phenomenon. As the austenite grain size of the sample annealed at 900 °C is lower than the initial annealed one, the dislocation density inside grains reaches to the critical value with higher rates than the coarse-grained sample. So, the TRIP effect is seen at the early stages of the uniform plastic deformation region. The total elongation of 127 % in initial coarse-grained sample is achieved due to the occurrence of TRIP at the later stages of the uniform plastic deformation region. The lower elongation of 67 % for sample annealed at 900 °C compared with as received sample is due to the lower austenite mean grain size and also the occurrence of TRIP at the early stages of plastic deformation. It is also worth to note that the stage III hardening is not observed during tensile deformation of initial coarse grained (Fig. 5(d)) and annealed samples at 800 and 900 °C (Fig. 5(b,c)).

As previously explained by Flinn et al. [33], the stage III hardening is expected when the high levels of plastic deformation could be imposed on sample before the necking during tensile testing. In the case of the sample annealed at 700 °C, the microstructure just before tensile testing is composed of elongated austenite grains with the characteristics of the cold work state (Fig. 2(a)). So, the initial dislocation density is high enough to trigger dislocation annihilation process during tensile deformation. Whereas, in samples annealed at 800 and 900 °C and initial coarse grained one, the microstructure mainly consisted of equiaxed and recrystallized austenite grains with low levels of dislocation densities. Therefore, the dislocation density during tensile testing does not reach to a value for the annihilation process to occur extensively.

Conclusions

In the present investigation, the AISI 321 austenitic stainless steel was cold rolled with 80 % reduction and then annealed at 700, 800, and 900 °C for 15 min to produce different initial microstructures for subsequent analysis. Then, the work hardening behaviors of annealed samples were analyzed using room temperature tensile testing. The main results are as follows:

1. In the Holomon analysis, all samples with different initial microstructures showed two-stage work hardening behavior. The absence of the stage I hardening in all samples and

the stage III hardening in sample annealed at 900 °C and as received specimen was confirmed by this analysis.
2. The stage III of hardening is not apparent in sample annealed at 900 °C and coarse grained one. The reason for this observation is that the density of dislocations in the sample at the final stages of the tensile testing does not reach to the critical value necessary for dynamic recovery to occur.
3. In the C-J analysis, the initial hardening stage, which is the indication of multiple slip at large grains, is not observed in the sample annealed at 700 °C for 15 min. At this annealing temperature, the microstructure is mainly consisted of elongated austenite grains with high density of dislocations which arrange in the form of dislocation cells and ultrafine grains resulted from martensite to austenite reversion. At other annealing conditions, the initial stage is observed due to the presence of large austenite grains in microstructures.
4. The stage III work hardening in the C-J analysis was observed only for the sample annealed at 700 °C. This is due to the high density of dislocations existed inside austenite grains before tensile testing.
5. The positive slop in the $\ln(d\sigma/d\varepsilon)$ vs. $\ln(\varepsilon)$ curves of the sample annealed at 900 °C and coarse grained one is attributed to the occurrence of austenite to martensite transformation (TRIP effect) which results in higher ductility and elongation to failure at these conditions.

CRediT authorship contribution statement

Mehdi Shaban Ghazani **:** writing – review & editing, writing – original draft, conceptualization, methodology; **Hesam Asghar Rezaei** **:** experimental design, sample preparation, investigation, analyses.

Conflict of interest

The authors declare that they have no conflict of interest.

References

1. Verma J, Taiwade RV. Effect of welding processes and conditions on the microstructure, Mechanical properties and corrosion resistance of duplex stainless steel weldments—A review. *J. Manuf. Process.* 2017;25: 134–152.
2. Kina AY, Souza VM, Tavares S, Pardal J, Souza J. Microstructure and intergranular corrosion resistance evaluation of AISI 304 steel for high temperature service. *Mater. Charact.* 2008;59(5): 651–655.
3. Singh R, Chattoraj I, Kumar A, Ravikumar B, Dey P. The effects of cold working on sensitization and intergranular corrosion behavior of AISI 304 stainless steel. *Metall. Mater. Trans. A.* 2003;34: 2441–2447.
4. Anita T, Pujar M, Shaikh H, Dayal R, Khatak H. Assessment of stress corrosion crack initiation and propagation in AISI type 316 stainless steel by electrochemical noise technique. *Corros. Sci.* 2006;48(9): 2689–2710.
5. Tiamiyu A, Eduok U, Szpunar J, Odeshi A. Corrosion behavior of metastable AISI 321 austenitic stainless steel: Investigating the effect of grain size and prior plastic deformation on its degradation pattern in saline media. *Sci. Rep.* 2019;9: 12116.
6. Lima A, Nascimento A, Abreu H, de Lima-Neto P. Sensitization evaluation of the austenitic stainless steel AISI 304L, 316L, 321 and 347. *J. Mater. Sci.* 2005;40: 139–144.
7. Pardo A, Merino M, Coy A, Viejo F, Carboneras M, Arrabal R. Influence of Ti, C and N concentration on the intergranular corrosion behaviour of AISI 316Ti and 321 stainless steels. *Acta. Mater.* 2007;55(7): 2239–2251.
8. Yanhui Z, Haitao M, Lai W, Changhai S, Chao G. Effect of solution treatment on microstructures and mechanical properties of AISI 321 service. *Acta Metall. Sin. (Engl. Lett.).* 2011;24(3): 243–248.

9. Yu C, Kao P, Chang C. Transition of tensile deformation behaviors in ultrafine-grained aluminum. *Acta. Mater.* 2005;53(15): 4019–4028.
10. Rybin VV, Ushanova EA, Zolotorevsky NY, Ermakova NY. Study of copper work-hardening behavior on a single sample experienced inhomogeneous dynamic deformation. *Materials Physics and Mechanics.* 2015;24(3): 253–258.
11. Y. Wang, E. Ma, Strain hardening, strain rate sensitivity, and ductility of nanostructured metals. *Mat. Sci. Eng. A.* 2004;375–377: 46–52.
12. Dini G, Najafizadeh A, Ueji R, Monir-Vaghefi S. Tensile deformation behavior of high manganese austenitic steel: The role of grain size. *Mater. Design.* 2010;31(7): 3395–3402.
13. Ma E. Instabilities and ductility of nanocrystalline and ultrafine-grained metals. *Scr. Mater.* 2003;49(7): 663–668.
14. Wang Y, Ma E. Three strategies to achieve uniform tensile deformation in a nanostructured metal. *Acta. Mater.* 2004;52(6): 1699–1709.
15. Zhang W, Wu J, Wen Y, Ye J, Li N. Characterization of different work hardening behavior in AISI 321 stainless steel and Hadfield steel. *J. Mate. Sci.* 2010;45: 3433–3437.
16. Rezaei H, Ghazani MS, Eghbali B. Effect of post deformation annealing on the microstructure and mechanical properties of cold rolled AISI 321 austenitic stainless steel. *Mat. Sci. Eng. A.* 2018;736: 364–374.
17. Meyers MA, Mishra A, Benson DJ. Mechanical properties of nanocrystalline materials. *Prog. Mater. Sci.* 2006;51(4): 427–556.
18. Zheng M, Li ZM. Strain-Hardening effect on critical strain assessment of pipe plastic bending at buchling. *Materials Physics and Mechanics.* 2020;44(1): 48–60.
19. Shin JH, Jeong J, Lee JW. Microstructural evolution and the variation of tensile behavior after aging heat treatment of precipitation hardened martensitic steel. *Mater. Charact.* 2015;99: 230–237.
20. Kosaka N, Funakawa Y. Work hardening in ferritic steel containing ultra-fine carbides, *ISIJ Int.* 2016;56(2): 311–318.
21. Šesták B, Seeger A. The Relationship between the Work-Hardening of BCC and FCC Metals. *Phys. Status. Solidi. B.* 1971;43(1): 433–444.
22. Del Valle J, Carreño F, Ruano OA. Influence of texture and grain size on work hardening and ductility in magnesium-based alloys processed by ECAP and rolling. *Acta. Mater.* 2006;54(6): 4247–4259.
23. Rollett AD, Kocks U. A review of the stages of work hardening. *Solid State Phenom.* 1993;35–36: 1–18.
24. Gronostajski Z. The constitutive equations for FEM analysis. *J. Mater. Process. Technol.* 2000;106(1–3): 40–44.
25. Das D, Chattopadhyay PP. Influence of martensite morphology on the work-hardening behavior of high strength ferrite–martensite dual-phase steel. *J. Mater. Sci.* 2009;44: 2957–2965.
26. Umemoto M, Tsuchiya K, Liu Z, Sugimoto S. Tensile stress-strain analysis of single-structure steels. *Metall. Mater. Trans. A.* 2000;31(7): 1785–1794.
27. Colla V, De Sanctis M, Dimatteo A, Lovicu G, Solina A, Valentini R. Strain hardening behavior of dual-phase steels. *Metall. Mater. Trans. A.* 2009;40: 2557.
28. Kumar SS, Raghu T. Tensile behaviour and strain hardening characteristics of constrained groove pressed nickel sheets. *Mater. Design.* 2011;32(8–9): 4650–4657.
29. Afrin N, Chen D, Cao X, Jahazi M. Strain hardening behavior of a friction stir welded magnesium alloy. *Scr. Mater.* 2007;57(11): 1004–1007.
30. Reed-Hill R, Cribb W, Monteiro S. Concerning the analysis of tensile stress-strain data using log dσ/dεp versus log σ diagrams, *Metall. Mater. Trans. B.* 1973;4: 2665–2667.
31. Raabe D, Zhao Z, Mao W. On the dependence of in-grain subdivision and deformation texture of aluminum on grain interaction. *Acta. Mater.* 2002;50(17): 4379–4394.
32. Cai Z, Ding H, Xue X, Jiang J, Xin Q, Misra R. Significance of control of austenite stability and three-stage work-hardening behavior of an ultrahigh strength–high ductility combination transformation-induced plasticity steel. *Scr. Mater.* 2013;68(11): 865–868.
33. Flinn J, Field D, Korth GE, Lillo TM, Macheret J. The flow stress behavior of OFHC polycrystalline copper. *Acta. Mater.* 2001;49(11): 2065–2074.